ARTICLES

Luminescence Spectroscopy and Visible Upconversion Properties of Er^{3+} in ZnO Nanocrystals

Xin Wang, Xianggui Kong,* Guiye Shan, Yi Yu, Yajian Sun, Liyun Feng, Kefu Chao, Shaozhe Lu, and Yajun Li

Key Laboratory of Excited-State Process, Changchun Institute of Optics Fine Mechanics and Physics, Chinese Academy of Sciences, Changchun 130033, P. R. China

Received: May 8, 2004; In Final Form: August 4, 2004

Er^{3+}-doped ZnO nanocrystals with hexagonal wurtzite structure were prepared by addition of LiOH to Zn−O−Er precursors in ethanol. The well-known green hot band from the $^2H_{11/2} \rightarrow {}^4I_{15/2}$ transition in the 520 − 540 nm region and Stokes emissions were investigated. And the blue, green, and red upconversion emissions were observed from the annealed samples under near-infrared light (808 nm) excitation. The upconversion emission intensity ratio of the hypersensitive $^2H_{11/2} \rightarrow {}^4I_{15/2}$ to $^4S_{3/2} \rightarrow {}^4I_{15/2}$ transition (I_{530nm}/I_{550nm}) in the sample annealed at 400 °C is different from that in the sample annealed at 700 °C, which is attributed to the variation of the local structure around Er^{3+} ions. The upconversion emission spectra and the pump power dependence of the luminescence intensities are provided to explain the upconversion mechanisms. These results confirm that visible upconversion emissions of Er^{3+} in the ZnO nanocrystals are mainly produced via two-photon excited-state absorption (ESA) and energy transfer upconversion (ETU) processes.

Introduction

In recent years, rare-earth (RE) doped nanocrystals have attracted a great deal of attention due to particle-size dependent optical properties,[1−3] which lead to their potential application in phosphors,[1,4] display monitors,[5] optical communication,[6,7] and two-photon fluorescence imaging.[8] Furthermore, RE ions, especially trivalence erbium, are much suitable for the conversion of infrared to visible light (upconversion) due to a favorable electronic energy level structure. The excited states ($^4I_{9/2}$ and $^4I_{11/2}$) of Er^{3+} ion with long lifetimes can easily be populated with near-infrared (NIR) radiation. The availability of low-cost NIR laser diode brings much convenience for the realization of upconversion emissions. Moreover, upconversion emissions of Er^{3+}-doped nanocrystals have been achieved in different crystal structure hosts, such as cubic ZrO_2, Y_2O_3, Lu_2O_3, $BaTiO_3$;[7−15] tetragonal $La_2(MoO_4)_3$;[16] and anatase and rutile TiO_2.[8,17]

Fluorescence labeling is very useful practice in biological applications, such as immunoassay, DNA sequencing, and clinical diagnostics.[18−24] Ultrasensitive detection of nucleic acid marked with upconversion phosphors (UCP) has been reported by Rijke et al.[21] As fluorescence labeling material compared with conventional fluorophores (e.g., Cy5, TMR),[18,24] UCP with no photobleaching shows higher sensitivity and lower background, where high-luminescence efficiency and homogeneous nanometer size distribution are critically important for detection of biomolecules (protein, DNA, RNA) and immunoassay. This work is motivated by not only the purpose of the Er^{3+}-doped nanocrystals as UCP for fluorescence label but also the fundamental interest to better understand upconversion luminescence properties of different erbium hosts.

As a wide band-gap semiconductor and traditional phosphors material, ZnO has been extensively studied since 1950s.[25] Recently, electroluminescence of RE ions in polycrystalline ZnO obtained by sintering at high temperature of 1200 °C in air has been reported, whereas no photoluminescence arising from the RE^{3+} was observed due to RE ions locating near the grain boundaries of ZnO.[26] However, since a novel method of synthesizing ZnO colloids was applied,[27] the Stokes emissions of RE^{3+} in the ZnO nanocrystals have been reported by Spanhel et al.[28,29] and Liu et al.[30−31]

The research on Er^{3+}-doped ZnO nanoparticles has mainly focused on the Stokes luminescence properties during the past decades; very few works were reported about the upconversion luminescence.[28−31] To the best of our knowledge, the upconversion emissions of Er^{3+} in ZnO nanocrystals have not been reported in the literatures. In this work, the luminescence spectroscopy and visible upconversion emissions of Er^{3+} in the ZnO nanocrystals have been thoroughly investigated. The ratio of the upconversion luminescence intensity of the peak at 530 nm to that of the peak at 550 nm (I_{530nm}/I_{550nm}) in the samples annealed at 400 and 700 °C, respectively, is different. The difference of green upconversion emission spectral shape is due to the variation of the local structure around Er^{3+} ions site in the ZnO nanocrystals. It is also found that the annealing temperature plays an important role in the luminescence intensities and optical properties of Er^{3+} in the ZnO particles. Furthermore, the upconversion emission mechanism has been discussed in detail at the 4f electronic energy level scheme of Er^{3+} ion.

* To whom correspondence should be addressed. Tel: +86-431-6176313. Fax: +86- 431-4627031. E-mail: xgkong14@ciomp.ac.cn

10.1021/jp048021t CCC: $27.50
Published on Web 11/10/2004

Experimental Section

The Er^{3+}-doped ZnO colloidal suspension was prepared according to the method described by Spanhel et al.[27−29] and Liu et al.[30] with a slightly modification: In short, a 50 mL turbid ethanol suspension containing a mixture of 1.079 ± 0.001 g zinc acetate dihydrate (98$^+$%, Beijing Chemical) and 0.034 ± 0.001 g erbium acetate hydrate (99.9%, Aldrich) with a molar ratio Zn/Er ≈ 98:2 was refluxed while stirring for 180 min at about 80 °C. After this procedure, a clear Zn−O−Er precursor solution was obtained, and then cooled to room temperature. The precursor was hydrolyzed by addition of 0.29 g lithium hydroxide monohydrate powder (from Fluka) in an ultrasonic bath at 0 °C for 20 min. The mixture was filtered through a 0.1 μm glass fiber filter to remove the dust and insoluble residue. The colloid solution was precipitated when preferably less toxic hexane had been added.[32] ZnO nanoparticles were redispersed in ethanol and then separated from the ethanol by precipitation. This procedure had been repeated for several times to remove physisorbed ionic compounds on the surface of ZnO particles. The precipitates were dried at room temperature in a vacuum oven for 12 h. The dried ZnO particles were annealed in air at a series of different temperatures from 300 to 900 °C for 30 min. The final product was white powder.

The crystal phase of annealed samples was identified by powder X-ray diffraction (XRD). The XRD patterns of the different samples recorded with different temperatures were acquired using a Japan Rigaku D/max-rA X-ray diffractometer system with a monochromatized Cu Kα irradiation (λ = 1.5418 Å).

Stokes emission spectra of Er^{3+} in the ZnO nanocrystals were measured using a Jobin-Yvon LabRam Raman spectrometer system equipped with 600 and 1800 grooves/mm holographic gratings, and a peltier air-cooled CCD detector. Precise control of sample temperature (±0.1 °C) was achieved by means of a Linkam THMS600 temperature programmable heating/cooling microscope stage. The THMS stage was used in conjunction with a Linkam LNP cooling system when cooling. Samples were excited using a 488 nm line of Spectra-Physics Model 164 argon ion laser. The time-resolved luminescence investigations were performed at room temperature following excitation with a tuned 488 nm wavelength light from pulsed Nd:YAG optical parametric oscillator (OPO) laser. The signals corresponding to decay curves of the Stokes emissions from photomultiplier (Hamamatsu R928) attached in the spectrometer (Jobin-Yvon TRIAX550) were collected by a Tektronix TDS 3052 500 MHz digital real-time storage oscilloscope. Upconversion emission spectra were recorded with a Hitachi F-4500 luminescence spectrophotometer using an external 808 nm semiconductor solid laser (1W) as the excitation source.

Results and Discussion

Structural Investigations. Figure 1 illustrates the XRD patterns of the Er^{3+}-doped ZnO nanocrystals at various conditions. The positions and relative intensities of the diffraction peaks are in good agreement with the Joint Committee of Powder Diffraction Standards data (JCPDS No. 36-1451), showing that the main structure of the samples is of hexagonal wurtzite. The XRD patterns indicate the presence of highly crystalline ZnO nanocrystals without any amorphous component and other additional Er_2O_3 crystalline phase. In the range of 300−900 °C, no peak related to the second phase of ZnO was observed at the XRD patterns. Meanwhile, the diffraction peaks become stronger and sharper with the rise in annealing temperature, which implies the growth of nanoparticles. On the basis

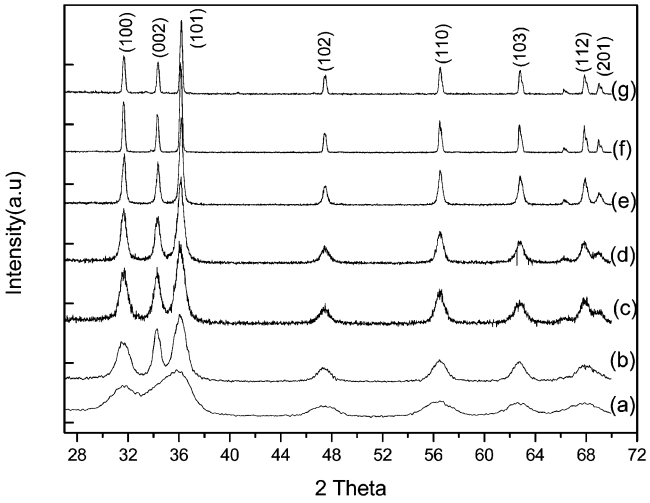

Figure 1. Powder X-ray diffraction patterns of the Er^{3+}-doped ZnO nanocrystals processed at various conditions: (a) dried at room temperature, and annealed at (b) 300, (c) 400, (d) 500, (e) 600, (f) 700, and (g) 800 °C.

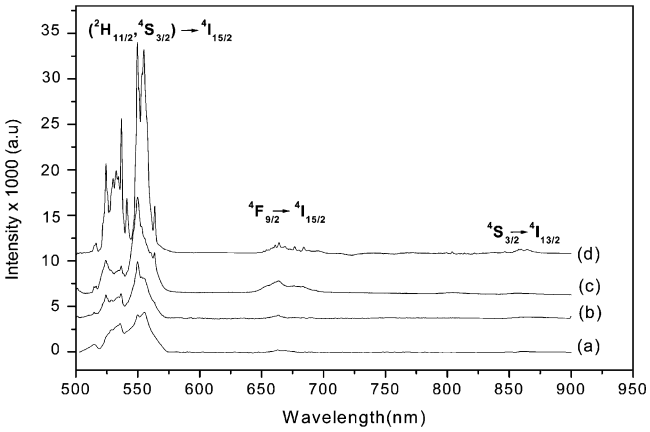

Figure 2. Room-temperature Stokes emissions of Er^{3+} in the ZnO nanocrystals annealed at (a) 400, (b) 500, (c) 600, and (d) 700 °C upon excitation at 488 nm.

of the XRD patterns, the average sizes of the ZnO nanoparticles can be estimated by the Debye−Scherrer's equation

$$D = K\lambda/\beta \cos \Theta \quad (1)$$

where D represents the average diameter of the particles, K = 0.89, λ is the wavelength of the Cu Kα radiation, Θ is the Bragg angle, and β is the corrected full width at half-maximum. The calculated results are about 3.4, 6.8, 48, and >80 nm for the different samples processed at room temperature (RT), 300, 500, and 700 °C, respectively.

Stokes Emission Spectroscopy. The room-temperature Stokes emission spectra of Er^{3+} in the ZnO nanocrystals under 488 nm excitation (excited directly into the $^4F_{7/2}$ level) are showed in Figure 2, where three distinct emission bands can be observed in the green, red, and NIR regions. Green emissions between 510 and 570 nm were assigned to the transitions from the $^2H_{11/2}$ and $^4S_{3/2}$ excited states to the $^4I_{15/2}$ ground state of Er^{3+} ion. Red emission was observed between 650 and 690 nm, corresponding to the $^4F_{9/2} \rightarrow {}^4I_{15/2}$ transition. Moreover, NIR emission was observed from the $^4S_{3/2} \rightarrow {}^4I_{13/2}$ transition in the range of 850−880 nm.[11] Obviously, the Stokes emission intensities were found to increase with the rise in annealing temperature from 400 to 700 °C (Figure 2a-d). Many fine structures observed in the Stokes emission spectra for the 700 °C annealed sample is

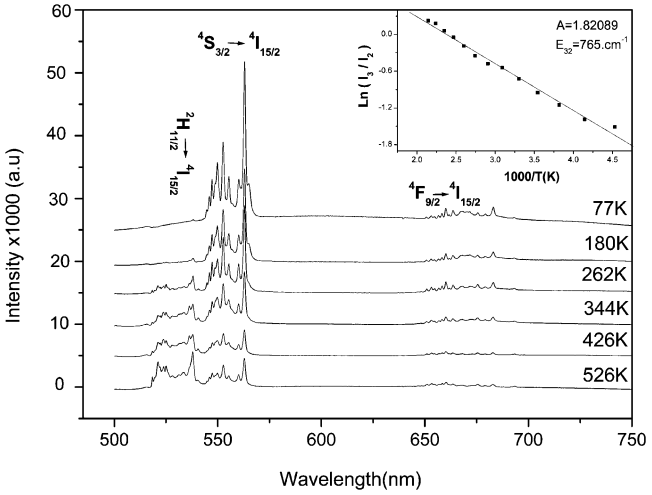

Figure 3. The measured temperature dependence of Stokes emission spectra for the sample annealed at 700 °C. Inset: Logarithm of the integrated intensity ratio of the $^2H_{11/2} \rightarrow {}^4I_{15/2}$ to $^4S_{3/2} \rightarrow {}^4I_{15/2}$ transitions as a function of inverse absolute temperature (10^3/T).

attributed to the crystal field variation due to the modification of the Er^{3+} local structure.

It is displayed in Figure 3 that the measured temperature dependence of Stokes emissions for the 700 °C annealed sample in the 500−700 nm region under 488 nm excitation. At the liquid nitrogen temperature of 77 K, the emission from $^2H_{11/2} \rightarrow {}^4I_{15/2}$ transition was not observed, whereas both the emissions of the $^4S_{3/2} \rightarrow {}^4I_{15/2}$ and $^4F_{9/2} \rightarrow {}^4I_{15/2}$ transitions were clearly observed. As the measured temperature increased up to 180 K, the well-known green hot band corresponding to the $^2H_{11/2} \rightarrow I_{15/2}$ transition was just now seen. Following an increase of the measured temperature, the luminescence intensity of the $^2H_{11/2} \rightarrow I_{15/2}$ transition increased at the expense of the $^4S_{3/2} \rightarrow {}^4I_{15/2}$ transition, and the former transition was dominant compared with the latter one up to 426 K. As a feeding level of the population of the $^2H_{11/2}$ level, the $^4S_{3/2}$ level was depopulated with increasing the measured temperature. The thermalization of the $^2H_{11/2}$ level could be expressed by the following equation[33−34]:

$$\frac{I_3}{I_2} = A \exp\left(-\frac{\Delta E_{32}}{KT}\right) \tag{2}$$

where I_3 and I_2 are the integrated intensities of the transitions from the $^2H_{11/2}$ and $^4S_{3/2}$ excited states to the $^4I_{15/2}$ ground state, respectively, ΔE_{32} is the energy gap between the $^2H_{11/2}$ and $^4S_{3/2}$ level, K is Boltzmann constant, T is the absolute temperature, and A is given by the following equation

$$A = (W_{R3} g_3 h\nu_3)/(W_{R2} g_2 h\nu_2) \tag{3}$$

where W_{R3} and W_{R2} are the radiative probabilities of two transitions, g_3 and g_2 are the $(2J+1)$ degeneracies of $^2H_{11/2}$ and $^4S_{3/2}$ levels, and $h\nu_3$ and $h\nu_2$ are the photon energies of the respective transitions from $^2H_{11/2}$ and $^4S_{3/2}$ levels to $^4I_{15/2}$ level. A straight line fitting the calculated values of $\ln(I_3/I_2)$ versus $1/T$ was obtained, whose slope had a value of 765 cm^{-1}, corresponding to the energy gap ΔE_{32} between the $^2H_{11/2}$ and $^4S_{3/2}$ levels (Figure 3, insert). The 765 cm^{-1} value is consistent with the thermal vibration energy of the crystal lattice at the temperature of 175 K, which implies the initial temperature point of the thermalization of the $^2H_{11/2}$ level, in good agreement with the experiment data of 180 K.

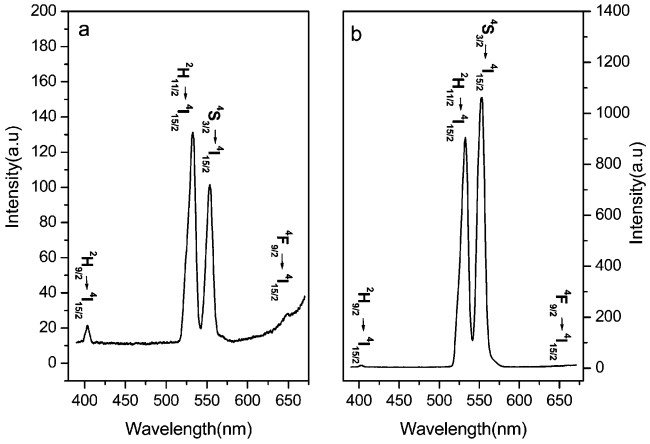

Figure 4. Upconversion luminescence spectra of Er^{3+} in the ZnO nanocrystals annealed at (a) 400 and (b) 700 °C under 808 nm excitation.

TABLE 1: Room-Temperature Decay Times for the ZnO:Er^{3+} Nanocrystals (annealed at 500, 600, and 700 °C) Obtained from the Decay Curves Fitted by a Monoexponential Model under 488 nm Pulsed Excitation

	decay times (μs) of ZnO:Er^{3+} nanocrystals		
	transition		
annealing temperature (°C)	$^2H_{11/2} \rightarrow {}^4I_{15/2}$	$^4S_{3/2} \rightarrow {}^4I_{15/2}$	$^4F_{9/2} \rightarrow {}^4I_{15/2}$
700	4.45	4.36	4.22
600	4.05	3.98	4.53
500	4.02	3.96	4.47

The room-temperature decay curves for the ($^2H_{11/2}$, $^4S_{3/2}$) $\rightarrow {}^4I_{15/2}$ and $^4F_{9/2} \rightarrow {}^4I_{15/2}$ transitions under 488 nm pulsed excitation could be fitted well using a monoexponential function for the samples annealed at all the temperatures mentioned above. The phenomenon could be explained on the basis of multiphonon relaxation, which is attributed to the presence of acetate and hydroxyl groups on the surface of the ZnO nanocrystals. The lifetimes are shown in Table 1, where the average lifetime of the green fluorescence is 4.14 μs. It is worth mentioning that the decay time of the green ($^4S_{3/2}$) excited state is shorter than that of the red ($^4F_{9/2}$) excited state for the samples annealed at the 500 and 600 °C. However, for the 700 °C annealed sample, the decay time of the $^4S_{3/2}$ level is longer than that of the $^4F_{9/2}$ level. In addition, the decay time of the $^4S_{3/2}$ level increases with raising the annealing temperature, while the opposite case occurs to the $^4F_{9/2}$ level.

Upconversion Luminescence Properties. Upon excitation with an 808 nm CW semiconductor laser at room temperature, the blue, green, and red upconversion emissions of Er^{3+} ions in the ZnO nanocrystals were observed. The upconversion luminescence spectra for two samples annealed at 400 and 700 °C, respectively, are shown in Figure 4, where four emission bands at approximately 405 nm, 530, 550, and 660 nm are assigned to $^2H_{9/2}$ to $^4I_{15/2}$, $^2H_{11/2}$ to $^4I_{15/2}$, $^4S_{3/2}$ to $^4I_{15/2}$, and $^4F_{9/2}$ to $^4I_{15/2}$ transitions, respectively. It is obvious that the upconverted green luminescence intensity increases remarkably with raising the annealing temperature up to 700 °C, and the luminescence is very bright to be seen with naked eyes. However, it should be mentioned here that both blue and red emission intensities are much weaker than the green one, and this was also observed in a similar system of the Y_2O_3:Er^{3+} nanocrystals at the level of dopant Er^{3+} concentration less than 2 mol % following excitation with 815 nm, where the red emission is relatively weak in comparison with green one.[9] It is noted that there is a great difference between the shapes of

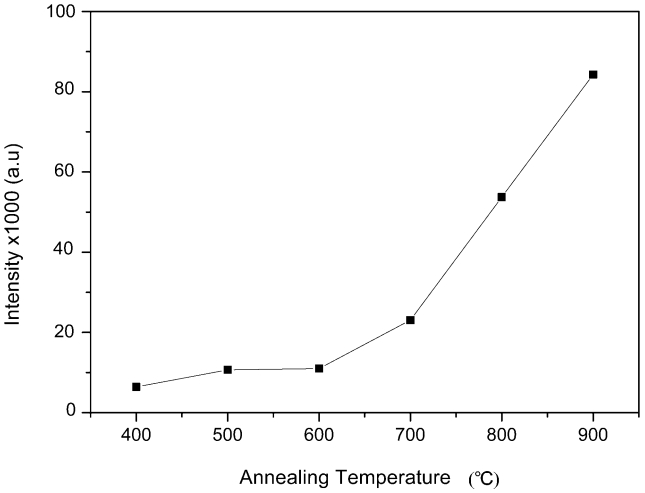

Figure 5. Effect of annealing temperature on the upconverted green luminescence intensities of Er^{3+} in the ZnO nanocrystals.

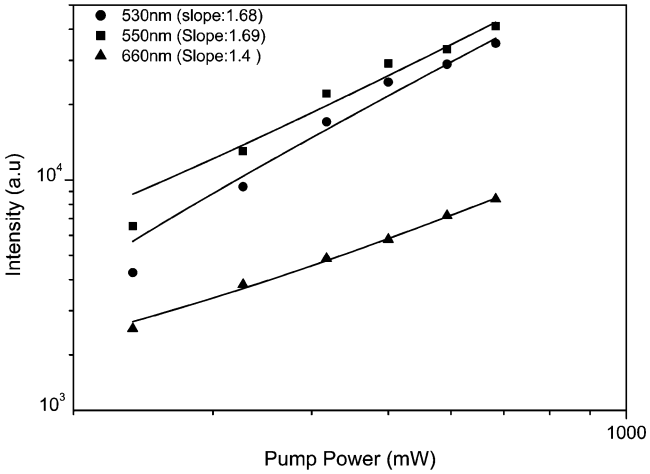

Figure 6. Pump power dependence of the upconverted green and red integrated intensities of Er^{3+} in the ZnO nanocrystals under 808 nm excitation.

upconversion luminescence spectra for 400 and 700 °C annealed samples. From Figure 4a, we can see the intensity of the emission peak at 530 nm is stronger than that of the emission peak at 550 nm in the sample annealed at 400 °C, while Figure 4b shows the opposite case occurring in the sample annealed at 700 °C. Similar phenomena have also been observed in the $La_2(MoO_4)_3$:Yb,Er nanocrysals at different sintering temperatures.[16] In fact, since a greater fraction of the erbium ions distributes on the surface than that in the interior of nanometer-scale particles, the doped erbium ions cause its local lattice distortion of the ZnO nanoparticle surfaces, and this influence on the overall distortion increases with decreasing the particle size. As a whole, the local environments of erbium ions become an isotropic coordination with higher symmetry, and therefore, the interaction between erbium ion and its surrounding crystal lattice becomes weaker. This could interpret that the emission from hypersensitive $^2H_{11/2} \rightarrow {}^4I_{15/2}$ transition is stronger than that from the $^4S_{3/2} \rightarrow {}^4I_{15/2}$ transition in the sample annealed at 400 °C. On the contrary, after annealing at the temperature higher than 400 °C, the changes of atomic coordination number around Er^{3+} and/or the Er−O bond lengths reduce the Er^{3+} local structure symmetries, whose degradation enhances the effects of crystal field in the host matrix. As a result of the reduced symmetries, the interaction between Er^{3+} ion and its surrounding crystal lattice becomes so intense as to decrease the population of hypersensitive $^2H_{11/2}$ energy level through nonradiative relaxation process. Consequently, the $^2H_{11/2} \rightarrow {}^4I_{15/2}$ transition is weaker than the $^4S_{3/2} \rightarrow {}^4I_{15/2}$ one in the sample annealed at 700 °C.

The upconversion efficiency is mainly determined by the nonradiative processes of the host lattice.[13] However, the multiphonon relaxation is easy to happen due to the presence of some organic groups with high energy vibrational quanta on the nanocrystal surface, and thus shortening the lifetime of intermediate level in contrast with that in the counterpart bulk. In general, the multiphonon relaxation rate is dependent on the energy gap between the emitting level and the next lower level as well as the highest phonon energy in the host.[9] As an oxide, ZnO has low phonon energy, and its Raman spectrum (data not shown) shows a peak at about 440 cm^{-1} assigned to the characteristic vibrational mode of Zn−O bond. When the annealing temperature increased from 400 to 900 °C, the green upconversion luminescence of Er^{3+} in the ZnO nanocrystals was greatly enhanced. Figure 5 shows the green upconversion emission intensities as a function of the annealing temperature in the range of 400−900 °C. Notably, with the annealing temperature raising from 700 to 900 °C, the green luminescence intensities are about four times enhanced. As discussed above, the growth of the ZnO particles occurs at 400−900 °C, which brings a reduction of its surface defects to reduce the pathways of nonradiative decay. In addition, both Kohls et al.[29] and Sakohara et al.[35] have reported the presence of O═C< and OH− bands from the Fourier transform infrared (FTIR) spectra for the ZnO nanoparticles. The O═C< and OH− bands from acetate and hydroxyl groups on the surface of ZnO particles have high vibration energy of approximately 1500 and 3350 cm^{-1}, respectively. The acetate and hydroxyl groups also have high multiphonon relaxation rates, which are similar to the carbonate and hydroxyl groups on the surface of nanocrystalline Y_2O_3:Er^{3+}.[13] Consequently, the active ions in the nanocrystalline material relax through the emission of phonons rather than the emission of photons, which is the reason the decay time of the $^4F_{9/2}$ level is longer than that of the $^4S_{3/2}$ level in the 500 and 600 °C annealed samples. However, the loss of acetate and hydroxyl groups reduced the multiphonon relaxation rate after high-temperature annealing. Therefore, the enhancement of the green upconversion emission intensities related to the annealing temperature is ascribed to two main factors: one is the growth of the ZnO particles, which induces a decrease of the number of surface defects in the host; the second is the loss in the amount of acetate and hydroxyl groups, which lowers the multiphonon relaxation rate.

Usually, the upconversion emission in the 4f electron level can be understood by several well-known mechanisms:[36,37](a) excited-state absorption (ESA); (b) energy transfer (ET); (c) photon avalanche (PA). To better understand the mechanisms, the upconversion luminescence intensities of green ($^2H_{11/2}$,$^4S_{3/2} \rightarrow {}^4I_{15/2}$) and red ($^4F_{9/2} \rightarrow {}^4I_{15/2}$) emission have also been measured as a function of the pump power. The photon avalanche process can hardly occur in our experiments since no inflection point has been observed in the power-dependence study.[38] As is well-known, the upconversion emission intensity I_{UP} is proportional to the nth power of the excitation intensity I_{IR}, i.e., $I_{UP} \propto I_{IR}^n$, where n is the number of IR photons required to convert a visible photon, and its value is obtained from the slope of the graph of $\ln(I_{UP})$ versus $\ln(I_{IR})$. A straight line fitting the data points was yielded a slope of 1.68 and 1.4 for the ($^2H_{11/2}$, $^4S_{3/2}$) $\rightarrow {}^4I_{15/2}$ and $^4F_{9/2} \rightarrow {}^4I_{15/2}$ transitions in all samples under investigation (shown in Figure 6), respectively, and high multiphonon relaxation rate induced these slopes deviating from

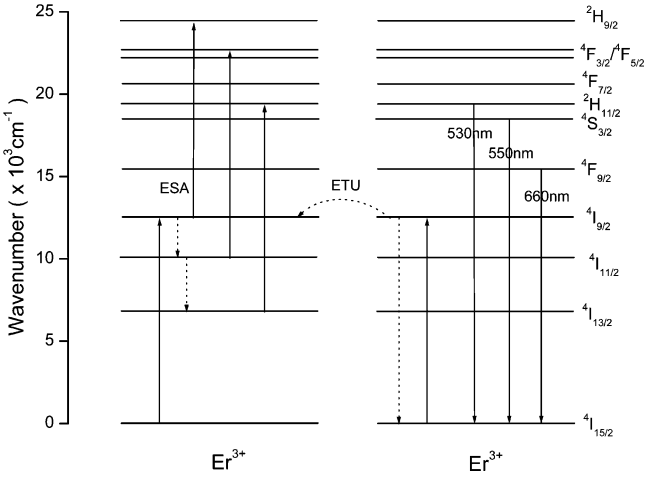

Figure 7. Schematic energy levels diagram of Er^{3+} ion in the ZnO nanocrystals and two-phonon excited-state absorption (ESA) and energy transfer upconversion (ETU) processes.

2. Therefore, we propose that a two-photon process was involved in the upconversion mechanism responsible for the blue, green, and red emission. In other words, two IR excitation photons are absorbed to produce a visible photon.

The mechanism of upconversion emission of Er^{3+} has been well established in the literature.[39,40] Therefore, the upconversion mechanisms proposed for the visible emission of Er^{3+} in the ZnO nanocrystals are shown in Figure 7. The dominant mechanisms are excited-state absorption (ESA) and energy transfer upconversion (ETU). The ESA involves only a single ion, whereas ETU involves two closely neighboring ions. The upconverted luminescence intensity in the two processes usually varies quadratically with the pump power, while varies linearly for the ESA and quadratically for the ETU process with the dopant rare earth ions concentration.[13] When the Er^{3+} ion at the $^4I_{9/2}$ level is excited by the ground-state absorption (GSA) process from the $^4I_{15/2}$ level under 808 nm excitation, the initial $^4I_{9/2}$ level population decay by a rapid multiphonon relaxation down to the $^4I_{11/2}$ and $^4I_{13/2}$ levels, with a portion of population in the $^4I_{13/2}$ level deriving from the $^4I_{11/2}$ level by relaxation. Under this excitation condition, the excited ions at the $^4I_{11/2}$ and $^4I_{13/2}$ level are excited to the $^4F_{3/2}$ and $^2H_{11/2}$ level via an ESA process, respectively. Since the lifetime of the lower energy $^4I_{13/2}$ excited state is longer than that of the $^4I_{11/2}$ excited state, the $^2H_{11/2} \leftarrow {}^4I_{13/2}$ transition can occur more easily in the system. The Er^{3+} ions at the terminal states of $^4F_{3/2}$ and $^2H_{11/2}$ nonradiatively decayed to the $^4S_{3/2}$ and $^4F_{9/2}$ states. The Er^{3+} energy level diagram reveals that there exists the $^2H_{9/2}$ energy level, which could be populated by resonant $^2H_{9/2} \leftarrow {}^4I_{9/2}$ transition following absorption of a second photon. The weak emission band locating at 390−410 nm is assigned to the transition from the $^2H_{9/2}$ level to the $^4I_{15/2}$ level. However, the two independent processes, ET and ESA, can occur simultaneously. It is well-known that the energy transfer can play an important role in the contribution to the upconversion luminescence when the dopant ions concentration in the nanometer material reaches a certain level of more than 1.0 mol %. Under 808 nm excitation, two closely neighboring Er^{3+} ions are excited to the $^4I_{9/2}$ intermediate state. One Er^{3+} ion in the $^4I_{9/2}$ state returns nonradiatively to the $^4I_{15/2}$ ground state, whose energy is transferred to neighboring Er^{3+} ion in the $^4I_{11/2}$ ($^4I_{13/2}$) state, and then the neighboring Er^{3+} ion is excited to the $^4F_{3/2}$ ($^2H_{11/2}$) state through the following channels: ($^4I_{9/2}$, $^4I_{11/2}$) → ($^4I_{15/2}$, $^4F_{3/2}$) and ($^4I_{9/2}$, $^4I_{13/2}$) → ($^4I_{15/2}$, $^2H_{11/2}$). Transition from the $^2H_{11/2}$ excited state to the $^4I_{15/2}$ ground-state results in the emission around 530 nm. This emission around 550 nm is assigned to the radiation transition from the $^4S_{3/2}$ to $^4I_{15/2}$ level. The $^4F_{9/2} \rightarrow {}^4I_{15/2}$ transition produces the red emission around 660 nm.

Conclusions

In this paper, the NIR to visible upconversion luminescence of Er^{3+} in the ZnO nanocrystals under 808 nm excitation has been investigated. After directly exciting into the $^4F_{7/2}$ level with a wavelength of 488 nm, the green hot band from the $^2H_{11/2} \rightarrow {}^4I_{15/2}$ transition and the Stokes emissions have been observed in the Er^{3+}-doped ZnO nanocrystals. The lifetime of green fluorescence is about 4.14 μs from a monoexponential fit of the decay curves for the ($^2H_{11/2}$,$^4S_{3/2}$) → $^4I_{15/2}$ transition under 488 nm pulsed excitation. The variation of the local structure around Er^{3+} ions occurred to the change of upconversion luminescence spectral shape for the two samples annealed at 400 and 700 °C, respectively. The green upconversion luminescence of Er^{3+} in the ZnO nanocrystals was enhanced along with the annealing temperature increasing from 400 to 900 °C. Power-dependence studies suggest that the green ($^2H_{11/2}$/$^4S_{3/2} \rightarrow {}^4I_{15/2}$) and red ($^4F_{9/2} \rightarrow {}^4I_{15/2}$) upconversion emissions occurred via a two-photon process. Furthermore, the upconversion mechanisms in the ZnO:Er^{3+} nanocrystals were also discussed in detail.

Acknowledgment. The authors gratefully acknowledge the financial support of the Major Foundation of Chinese Academy of Sciences (Grant No. 2002CD713802), the National High Technology Development Program (Grant No. 2002AA302203), and the National Nature Science Foundation of China (Grant No.10274083). The authors are also grateful to Professor Andong. Xia (Institute of Chemistry Chinese Academy of Sciences) for helpful discussions.

References and Notes

(1) Soo, Y. L.; Huang, S. W.; Ming, Z. H.; Kao, Y. H.; Smith, G. C.; Goldburt, E. T.; Hodel, R.; Kulkarni, B.; Veliadis, J. V. B.; Bhargava, R. N. *J. Appl. Phys*. **1998**, *83*, 5404.

(2) Goldburt, E. T.; Kulkarni, B.; Bhargava, R. N.; Taylor, J.; Libera, M. *J. Lumin*. **1997**, *72*−*74*, 190.

(3) Williams, D. K.; Yuan, H.; Tissue, B. M. *J. Lumin*. **1999**, *83*−*84*, 297.

(4) Tissue, B. M. *Chem. Mater*. **1998**, *10*, 2837.

(5) Mehta, A.; Thundat, T.; Barnes, M. D.; Chhabra, V.; Bhargava, R.; Bartko, A. P.; Dickson, R. M. *Appl. Optics*. **2003**, *42*, 2132.

(6) Zhang, H. X.; Kam, C. H.; Zhou, Y.; Han, X. Q.; Buddhudu, S.; Xiang, Q.; Lam, Y. L.; Chan, Y. C. *Appl. Phys. Lett*. **2000**, *77*, 609.

(7) Patra, A.; Friend, C. S.; Kapoor, R.; Prasad, P. N. *J. Phys. Chem. B* **2002**, *106*, 1909.

(8) Patra, A.; Friend, C. S.; Kapoor, R.; Prasad, P. N. *Chem. Mater* **2003**, *15*, 3650.

(9) Capobianco, J. A.; vetrone, F.; Christopher Boyer, J.; Speghini, A.; Bettinelli, M. *J. Phys. Chem. B* **2002**, *106*, 1181.

(10) Vetrone, F.; Christopher Boyer, J.; Capobianco, J. A.; Speghini, A.; Bettinelli, M. *J. Phys. Chem. B* **2003**, *107*, 1107.

(11) Vetrone, F.; Christopher Boyer, J.; Capobianco, J. A.; Speghini, A.; Bettinelli, M. *Chem. Mater*. **2003**, *15*, 2737.

(12) Tessari, G.; Bettinelli, M.; Speghini, A.; Ajò, D.; Pozza, G.; Depero L. E.; Allieri, B.; Sangaletti, L. *Appl. Surf. Sci*. **1999**, *144*−*145*, 686.

(13) Vetrone, F.; Christopher Boyer, J.; Capobianco, J. A. *J. Phys. Chem. B* **2002**, *106*, 5622.

(14) Capobianco, J. A.; Vetrone, F.; Boyer, J. C.; Speghini, A.; Bettinelli, M. *Opt. Mater*. **2002**, *19*, 259.

(15) Zhang, H. X.; Kam, C. H.; Zhou, Y.; Han, X. Q.; Buddhudu, S.; Lam, Y. L. *Opt. Mater*. **2000**, *15*, 47.

(16) Yi, G. S.; Sun, B. Q.; Yang, F. Z.; Chen, D. P.; Zhou, Y. X.; Cheng, J. *Chem. Mater*. **2002**, *14*, 2910.

(17) Bahtat, A.; Bouazaoui, M.; Bahtat, M.; Garapon, C.; Jacquier, B.; Mugnier, J. *Non-Cryst. Solids*. **1996**, *202*, 16.

(18) Chan, W. C.; Nie, S. *Science* **1998**, 281, 2016.
(19) Mattoussi, H.; Mauro, J. M.; Goldman, E. R.; Anderson, G. P.; Sundar, V. C.; Mikulec, F. V.; Bawendi, M. G. *J. Am. Chem. Soc*. **2000**, *122*, 12142.
(20) Santra, S.; Zhang, P.; Wang, K. M.; Tapec, R.; Tan, W. H. *Anal. Chem*. **2000**, *72*, 5748.
(21) Rijke, F. V. D.; Zijlmans, J.; Li, S.; Vail. T.; Raap, A. K.; Niedbala, R. S.; Tanke, H. *J. Nat. Biotechnol*. **2001**, *19*, 273.
(22) Hampl, J.; Hall, M.; Mufti, N. A.; Yao, Y. M.; Macquee, D. B.; Wright, W. H.; Cooper, D. E. *Anal. Biochem*. **2001**, *288*, 176.
(23) Zijlmans, H. J. M. A. A.; Bonnet, J.; Burton, J.; Kardos, K.; Tail, T.; Niedbala, R. S.; Tanke, H. J. *Anal. Biochem*. **1999**, *267*, 30.
(24) Grunwell, J. R.; Glass, J. L.; Lacoste, T. D.; Deniz, A. A.; Chemla, D. S.; Schultz, P. G. *J. Am. Chem. Soc*. **2001**, *123*, 4295.
(25) Dijken, A.; Meulenkamp, E. A.; Vanmaekelbergh, D.; Meijerink, A. *J. Phys. Chem. B* **2000**, 104, 1715.
(26) Bachir, S.; Kossanyi, J.; Sandouly, C.; Valat, P.; Ronfard-Haret, J. C. *J. Phys. Chem.* **1995**, *99*, 5674.
(27) Spanhel, L.; Anderson, M. A. *J. Am. Chem. Soc*. **1991**, *113*, 2826.
(28) Schmidt, T.; Müller, G.; Spanhel, L.; Kerkel, K.; Fouchel, A. *Chem. Mater*. **1998**, *10*, 65.
(29) Kohls, M.; Bonanni, M.; Spanhel, L. Su, D. S.; Giersig, M. *Appl. Phys. Lett*. **2002**, 81, 3858.
(30) Liu, S. M.; Liu, F. Q.; Guo, H. Q.; Zhang, Z. H.; Wang, Z. G. *Phys. Lett. A* **2000**, *271*, 128.
(31) Liu, S. M.; Liu, F. Q.; Wang, Z. G. *Chem. Phys. Lett*. **2000**, *343*, 489.
(32) Meulenkamp, E. A. *J. Phys. Chem. B* **1998**, *102*, 5566.
(33) Shinn, M. K.; Sibley, W. A.; Drexhage, M. G.; Brown, R. N. *Phys. Rev. B* **1983**, *27*, 6635.
(34) Xu, W.; Dai, S.; Toth, M.; Del Cul, G. D.; Peterson, J. R. *J. Phys. Chem*. **1995**, *99*, 4447.
(35) Sakohara, S.; Ishida, M.; Anderson, M. A. *J. Phys. Chem. B* **1998**, *102*, 10169.
(36) Bloembergen, N. *Phys. Rev. Lett.* **1959**, *2*, 84.
(37) Chivian, J. S.; Case, W. E.; Eden, D. D. *Appl. Phys. Lett*. **1979**, *35*, 124.
(38) Joubert, M. F.; Guy, S.; Jacquier, B. *Phys. Rev. B* **1993**, *48*, 10031.
(39) Tsuda, M.; Soga, K.; Inoue, I. S.; Makishima, A. *J. Appl. Phys*. **1999**, *85*, 29.
(40) Kanoun, A.; Jaba, N.; Mejri, H.; Maaref, H.; Selmi, A. *Phys. Stat. Sol*. **2001**, *188*, 1145.